ground water

Laboratory and Numerical Investigation of Flow and Transport Near a Seepage-Face Boundary

by M.J. Simpson[1], T.P. Clement[1,2,3] and T.A. Gallop[1]

Abstract

Laboratory and numerical modeling investigations were completed to study the unconfined ground water flow and transport processes near a seepage-face boundary. The laboratory observations were made in a radial sand tank and included measurements of the height of the seepage face, flow velocity near the seepage face, travel time distribution of multiple tracer slugs, and streamlines. All the observations were reliably reproduced with a three-dimensional, axi-symmetric, variably saturated ground water flow model. Physical data presented in this work demonstrate and quantify the importance of three-dimensional transport patterns within a seepage-face zone. The results imply that vertically averaged flow models that employ Dupuit approximations might introduce error in the analysis of localized solute transport near a seepage-face boundary. The experimental dataset reported in this work will also be of interest for those who are attempting to validate a numerical algorithm for solving ground water and contaminant discharge patterns near a surface-water boundary.

Introduction

Seepage-face boundaries are common features of unconfined ground water flow. These boundaries exist at the intersection of an unconfined aquifer and a surface water body such as a lake, river, or wetland. The existence of a seepage-face boundary is necessary to provide a physical transition between the internal water-table boundary and the external equipotential boundary when an unconfined aquifer intersects a surface water body (Bear 1972). In the vicinity of a seepage-face boundary, the phreatic surface normally rises above the elevation of the external surface water level, thereby creating an interface at atmospheric pressure where the fluid exits the porous medium.

The impact of seepage-face boundaries on the ground water flow and transport characteristics in an unconfined aquifer can be significant as the ground water velocities near the seepage face can be high (Vachaud and Vauclin 1975; Clement et al. 1996). This is because the seepage face is a sharp interface that separates the internal saturated zone where the fluid pressure is positive and the external seepage zone where the pressure is zero. Despite its importance, traditional solutions of unconfined flow problems routinely ignore the existence of seepage-face boundaries because of the difficulty of incorporating the mathematical description of the boundary in the analytical solution of the problem. In addition, several commonly used ground water models such as MODFLOW, MT3D, and RT3D do not explicitly consider the presence of seepage-face boundaries (Zheng and Bennett 2002; Clement 1997).

Seepage faces are formed due to the dominance of three-dimensional flow patterns near an outflow boundary (Clement et al. 1996). Therefore, if we are to gain a better insight into the influence of seepage faces on the ground water flow and solute transport processes, we need to better understand the nature of the three-dimensional ground water velocity field near the outflow boundary. Laboratory sand tank models are useful research tools to visualize the velocity field under various outflow conditions. Several investigators have used sand tank experiments to better understand the processes of ground water flow and solute transport in porous media systems. For example, radial flow tanks have been used to demonstrate the ground water flow characteristics about a pumping well (Wyckoff et al. 1932; Boulton 1951; Hall 1955). Sand tanks have also been

[1] Centre for Water Research, The University of Western Australia, Nedlands, 6907 Australia

[2]Department of Civil Engineering Auburn University, AL 36849

[3]Corresponding author: fax (334) 844–6290; clement@eng.auburn.edu

Received March 2002, accepted January 2003.

used to study ground water flow in Cartesian systems; for example, Luthin and Day (1955) studied the impact of unsaturated flow in a sand tank equipped with tensiometers to detect potential gradients within the unsaturated zone. Their work concluded that unsaturated flow could contribute to the total flow transmitted through unconfined systems. Laboratory models have also been used specifically to characterize the flow near a seepage-face boundary; for example, Chapman (1957) used a sand tank to generate data concerning the height of seepage faces so that a numerical method to determine the seepage-face height could be evaluated. Vauclin et al. (1975) conducted a series of tests in a Cartesian box to investigate the formation of seepage faces under transient conditions; the laboratory results were compared with results from a numerical model that aimed to replicate the physical observations. Oostrom et al. (1992) used a Cartesian sand tank model to investigate density-dependent solute transport processes in unconfined aquifers. Despite the widespread use of physical models since the early 1930s, there is still much to be learnt by observing ground water flow in laboratory scale models. For example, Silliman et al. (2002) recently used a Cartesian sandbox to qualitatively assess the importance of solute transport near the capillary fringe in unconfined flow systems. This work was primarily concerned with making a visual record of the movement of solutes through the unsaturated capillary zone by observing the movement of dye slugs within the laboratory model.

In addition to using laboratory scale models, investigators have often used mathematical models to develop a quantitative understanding of fluid flow and solute transport under unconfined conditions (Neuman 1973; Cooley 1983; Shamsai and Narasimhan 1991; Clement et al. 1994). In the ground water literature, three types of mathematical models are available for solving unconfined flow problems. Listed in the order of increasing complexity they are: the Dupuit-Forchheimer model (commonly known as the Dupuit model), the fully saturated three-dimensional model, and the variably saturated three-dimensional model (Clement et al. 1996). Note in Clement et al. (1996) the last two models were referred to as two-dimensional models and they describe Cartesian flow in the x and z (horizontal and vertical) directions while assuming a unit thickness in the y (lateral) direction.

The Dupuit model is based on a one-dimensional approximation of the governing flow equation that accounts only for saturated flow processes after ignoring the resistance to vertical flow (Bear 1972; Haitjema 1995). Because the governing equation is a depth-averaged one-dimensional expression, the Dupuit model cannot predict the existence of seepage faces. Despite this limitation, the simplicity of this approach has led to its widespread use for solving unconfined flow problems. It should be acknowledged that the Dupuit model performs adequately for many field-scale applications where the horizontal length-scale dominates.

The fully saturated three-dimensional model accounts for the three-dimensional nature of fluid flow, but it ignores the existence of the unsaturated zone. Application of this model is usually restricted to employing numerical approximations, such as the boundary integral method (Liggett and Liu 1983; Lee and Leap 1997). The variably saturated three-dimensional model incorporates both the three-dimensional nature of flow and the unsaturated flow processes. The variably saturated modeling approach also relies heavily on making numerical approximations to the governing equations (Cooley 1983; Clement et al. 1994). Clement et al. (1996) provided a detailed comparative analysis of these three models and discussed their relative merits.

Models are useful tools for identifying various hydrologic factors that affect ground water and solute discharge fluxes into sensitive surface water bodies, such as lakes and wetlands. The analysis of solute migration near a ground water/surface water interface, where seepage faces are usually formed, requires a detailed knowledge of the velocity field at the interface. Understanding the velocity field near a seepage-face interface is critical, because the seepage-face dynamics control the vertical distribution of ground water flow along the interface. Under strong gradient conditions, seepage faces control the spatial distribution of ground water input and transport of pollutants/nutrients into a surface water body, thereby determining the ecological function of the receiving waters (Tobias et al. 2001; Westbrook et al. 2000). In addition, the export of nutrients from watersheds to surface water bodies can be strongly controlled by the formation of large-scale seepage zones known as the riparian zone (Hauxwell et al. 2001). Seepage faces can also affect contaminant transport towards a pumping well; this can be particularly important when a pumping well is used for capturing contaminant plumes emanating from light non-aqueous phase liquid sources (Waddill and Parker 1997). Therefore, in many problems, it is imperative to have an accurate understanding of the ground water velocity field near the seepage-face boundary before any investigation into the localized fate and transport of dissolved chemical species near a seepage face can be completed with some level of certainty.

The objective of this work was to study the ground water flow and transport characteristics in an unconfined aquifer near a seepage-face boundary. A physical sand tank model was used to investigate unconfined flow dynamics in a radial system near a pumping well. The data from the laboratory experiments were modeled using a three-dimensional, axi-symmetric numerical model. The overall aim was to use the data collected from both physical and numerical experiments to develop a better understanding of the role that seepage faces play in controlling the transfer of ground water and dissolved solutes from unconfined aquifers into receiving water.

Laboratory Methods

A physical model of a radial flow system was used in this investigation to observe ground water flow and solute transport characteristics near a seepage face. The radial geometry has several practical advantages; first, physical modeling of ground water flow is made simpler in a radial domain because radial flow is relatively insensitive to unsaturated flow parameters (Clement et al. 1996). Radial problems are characterized by large volumes of flow transmitted through the saturated zone; consequently, the flow

contribution through the unsaturated zone is relatively less important when compared to an equivalent Cartesian flow system. Hence the overall flow dynamics of a radial flow system are relatively insensitive to the unsaturated flow properties of the porous medium (Clement et al. 1996). Second, the length of seepage faces are more pronounced in radial systems due to the converging nature of flow (Shamsai and Narasimhan 1991; Clement et al. 1996). Finally, radial systems have direct application to field-scale problems that involve pumping from unconfined aquifers.

Details of the Aquifer Model

The physical model used in this study is a 15-degree sector radial sand tank. The tank is 100 cm in height, with a distance of 130 cm between the centers of the inlet and outlet chambers. Figures 1 and 2 show photographs of the side and top views of the sand tank, respectively. The design of the radial tank was developed based on the details of the physical models described by Wyckoff et al. (1932) and Hall (1955).

The physical model has three chambers: The inlet chamber (which is used as the upstream constant-head boundary), the porous medium chamber (the unconfined aquifer), and the outlet chamber (downstream constant-head boundary or the pumping well). The inlet chamber was a cylindrical tank with an internal diameter of 40 cm. The internal diameter of the downstream well was 20 cm. Note that in this study the radial coordinate r was measured from the center of the downstream well. The model was constructed of plexiglass with a metal frame used to support the structure. Two thin plexiglass dividers were used to separate the inlet and outlet chambers from the main porous media chamber (or the aquifer). The dividers were perforated to allow the passage of fluid from the inflow chamber into the porous medium chamber, and then from the porous medium chamber into the downstream well. Standpipes installed in both the inlet chamber and downstream well were used to control the water level (hydraulic head). A grid of manometers located in the back of the tank was used to observe the pressure distribution within the laboratory aquifer.

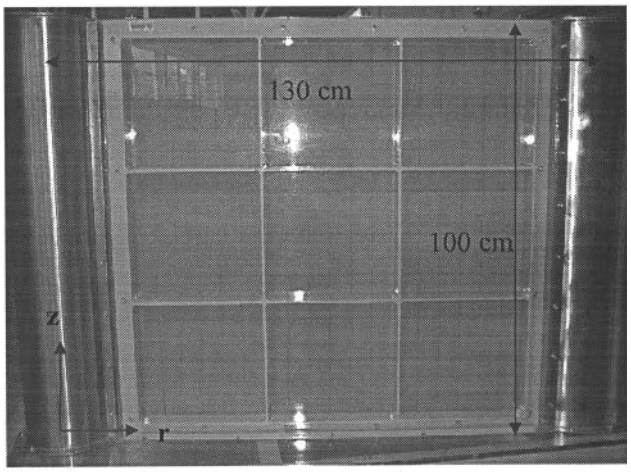

Figure 1. Side view of the laboratory aquifer.

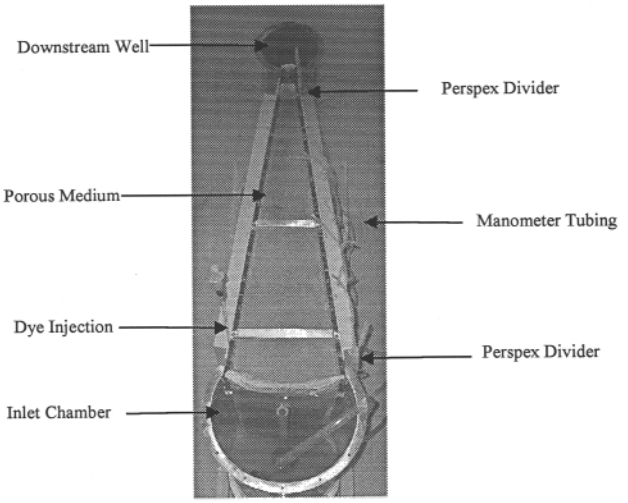

Figure 2. Top view of the laboratory aquifer.

The porous medium used in the experiments was clean sand, manufactured by Cook Industrial Minerals, Perth, Australia. The sand was uniform with a mean grain size of 1 mm. The sand was packed into the tank using a wet packing strategy to minimize packing heterogeneities and entrapment of air within the porous medium (Oostrom et al. 1992; Olivera et al. 1996).

Physical Measurements

The overall hydraulic conductivity of the tank was estimated by using an in situ technique (Oostrom et al. 1992). The length of the seepage face was directly estimated by measuring the highest elevation on the downstream boundary where the fluid exited the porous medium. The measurement of this elevation was obtained by injecting a slug of brightly colored dye upstream of the outflow boundary such that we could physically observe the maximum height when the dye crossed the boundary.

The vertical distribution of the horizontal velocity near the outflow boundary was measured to characterize the influence of the seepage-face boundary upon the internal velocity field. This was achieved by injecting dye slugs at ~5 cm upstream from the outflow boundary. The dye slugs were injected into the porous media chamber using a fine-tipped syringe (Figure 2). The time taken for the dye slugs to travel toward the outflow boundary was recorded and used to estimate the horizontal velocity profile.

A series of travel time measurements were also made to allow the analysis of solute-transport characteristics near the seepage face. These measurements were also made by injecting a series of small slugs of dye into the porous medium chamber using a syringe. Five dye slugs were injected at different depths along the vertical section where r = 105 cm, and the time taken for the slugs to traverse an aquifer to a fixed section, where r = 15 cm, was recorded. These experiments also allowed tracking of the streamlines. The coordinates of the streamlines were determined by simply recording the position of the center of mass of the slugs as they were transported through the aquifer. The streamline data were later used to characterize the spatial distribution of solutes.

Numerical Modeling Methods

The following three-dimensional, axi-symmetric, variably saturated flow equation was used to describe the steady-state flow in the physical model (Clement et al. 1994):

$$0 = \frac{1}{r}\frac{\partial}{\partial r}\left[rK(\theta)\frac{\partial \psi}{\partial r}\right] + \frac{\partial}{\partial z}\left[K(\theta)\frac{\partial \psi}{\partial z}\right] + \frac{\partial K(\theta)}{\partial z} \quad (1)$$

where ψ [L] is the fluid pressure head, K [LT^{-1}] is the hydraulic conductivity of the porous medium, θ is the water content of the porous medium, and r and z are the radial coordinates.

Numerical Solution Scheme

Equation 1 is a nonlinear partial differential equation and requires a numerical solution. The details of the numerical solution scheme are described in Clement et al. (1994). The numerical model can describe Dirichlet, Neumann and seepage-face boundary conditions, all of which are required to simulate the laboratory problem. The location of the seepage face was computed using the iterative search procedure described by Cooley (1983). The key features of the solution algorithm along with a description of how the original algorithm of Clement et al. (1994) was modified to solve the radial problem are summarized in Appendix A.

The results from the numerical solution to Equation 1 yield the pressure-head values at each point of the discretized domain. A uniform grid of Δr = 1.31 cm and Δz = 1.25 cm was used in this study to model the sand tank. The total number of nodes used in the radial direction was 77 and the number of nodes in the vertical direction was also 77. The nodal values of pressure head were used to calculate the fluid fluxes using the following Darcy equations:

$$q_r = -K\frac{\partial \psi}{\partial r}$$

$$q_z = -K\left[\frac{\partial \psi}{\partial z} + 1\right] \quad (2)$$

where q_r [LT^{-1}] and q_z [LT^{-1}] are the fluid fluxes in the radial and vertical directions.

Equation 2 was approximated using a central difference method for all the internal nodes in the numerical grid. For boundary nodes, either a forward or backward difference approximation was used. Once the distribution of the fluid flux was known, then the total inflow or outflow was determined by integrating the normal component of the discrete fluid flux over the area of the boundary.

Travel Time Analysis

The fluid velocity field within the domain was computed by dividing the nodal flux values by the nodal water content of the porous medium. Once the velocity field was obtained, the advective transport within the domain was simulated by the integration of the following ordinary differential equations that describe the path of a tracer particle within the velocity field (Güven et al. 1992):

$$v_r(r,z) = \frac{dr}{dt}$$

$$v_z(r,z) = \frac{dz}{dt} \quad (3)$$

where v_r [LT^{-1}] is the fluid velocity in the radial direction, v_z [LT^{-1}] is the fluid velocity in the vertical direction, and t [T] is the time. Because the output from the numerical solution of Equation 1 is discrete, it was possible to insert a particle at any location into the velocity field and then determine the velocity by linearly interpolating the discrete values (Güven et al. 1992). Integration of the differential system Equation 3 enabled the particles to be tracked forward in time, and this yielded the coordinates of various streamlines. Using these coordinates one could directly estimate the time taken for the particle to move from one position to another along any given streamline. The integration of the velocity Equation 3 was accomplished using the fourth-order Runge-Kutta algorithm with a constant time step (Press et al. 1992).

The variably saturated flow modeling approach used in this study has several numerical advantages over other options. First, the inclusion of the variably saturated portion of the flow domain avoids the need to deal with a moving boundary. Second, the variably saturated discretization can remain fixed over time and does not require remeshing as the solution converges. Finally, the inclusion of the variably saturated domain gives a more thorough description of all the physical processes occurring within the aquifer. Therefore, the numerical description adopted here is a convenient and thorough approach for analyzing the physical problem considered in this study.

Results and Discussion

Characterization of the Sand

The hydraulic conductivity of the sand tank was measured using an in situ technique described by Oostrom et al. (1992). This method was adopted because the overall hydraulic conductivity of the model depends on the packing conditions in the sand tank. Laboratory scale permeameter tests showed that the hydraulic conductivity of the sand used may vary from 86 m/day (in loosely packed columns) to 46 m/day (in densely packed columns), depending on the packing conditions. It was impossible to replicate the exact packing conditions of the sand tank in a small-scale soil column. Therefore, the column values were used as approximate estimates only to verify the measured in situ value. The general principle behind Oostrom et al.'s (1992) in situ measurement approach is that if the unsaturated contribution to the total flow rate is negligible, then the Dupuit discharge formula for unconfined flow can be used to compute the flow rate. For a radial system:

$$Q = \pi K\frac{(h_R^2 - h_w^2)}{log_e(r_R/r_w)} \quad (4)$$

where Q [L^{3}T^{-1}] is the total extraction rate from the well, h_R [L] and h_W [L] are the hydraulic head at the radius of

influence and the well casing respectively, and r_R [L] and r_W [L] are the radius of influence and the radius of the well casing. Note that Equation 4 assumes that the entire aquifer around the well is contributing to the flow. In this work, only a 15-degree sector was contributing to the total outflow, therefore the observed flow rate was ¼ of the Dupuit discharge. It is well known that the Dupuit formula can exactly predict the saturated flow through a porous medium even when there is a large seepage face present at the exit boundary (Polubarinova-Kochina 1962; Bear 1972; Keady et al. 1988). Further, in radial problems the contribution from the unsaturated flow is also relatively small (Clement et al. 1996).

Several flow measurements were made by varying the hydraulic gradient conditions. The hydraulic gradient was adjusted by holding the head in the upper reservoir at a fixed level and varying the head in the lower reservoir. The upstream reservoir head was set at 90 cm and the downstream head was varied between 70, 60, 40, and 20 cm. Note, in this paper, we use a nomenclature that uses the values of upstream and downstream fluid levels to refer to various hydraulic gradient experiments. For example, a 90:40 gradient experiment means that the flow corresponds to fluid levels of 90 cm in the inlet chamber and 40 cm in the downstream well.

A trial-and-error method was used to calibrate the flow predicted by the Dupuit discharge formula to the measured flow rates. The calibration analysis yielded an in situ hydraulic conductivity value of 67 m/day. In addition to the Dupuit formula, the numerical model was also used to compute the flow rate through the system for the estimated conductivity value of 67 m/day. Table 1 provides a summary of the flow rates predicted by the Dupuit discharge formula, the variably saturated numerical model, and the actual measured flow rate. It can be inferred from the table that the flow rates computed by the Dupuit formula are close to the observed flow rates. Further, the table also shows a good correspondence between the Dupuit flow and the flow predicted by the variably saturated numerical model. This result implies that the flow contribution from the unsaturated zone is relatively small, thereby justifying the use of Equation 4 to estimate the average hydraulic conductivity of the porous medium.

The measured saturated water content (porosity) of the sand was $\theta_s = 0.3$. The van Genuchten parameters used to related water content to the pressure head (see Appendix A) are $\alpha_v = 2.0\ m^{-1}$ and $n_v = 2.0$. These parameters represent medium-grained sand with fairly uniform pores (Wise et al. 1994). Clement et al. (1996) found that steady-state solutions to Equation 1 are relatively insensitive to the values of these parameters.

Seepage-Face Length

Experiments were conducted to determine the length of the seepage face formed at four different hydraulic gradients. The measured seepage-face lengths are compared to the lengths predicted by the numerical model in Table 2. The table shows that when the hydraulic gradient across the porous medium was decreased, the length of the seepage face also decreased. This is because higher hydraulic gradients forced a larger vertical gradient across the aquifer and thereby induced vertical flow about the exit boundary leading to the formation of a larger seepage face. Comparison of the seepage-face lengths predicted using the numerical model and those observed in the laboratory indicates that the numerical model can make accurate predictions of the seepage-face length.

Table 1
Comparison of Observed and Predicted Flow Rates Through the System

Head Gradient	90:20	90:40	90:60	90:70
$Q_{laboratory}$ (m^3/day)	2.74	2.56	1.76	1.14
Q_{Dupuit} (m^3/day)	2.82	2.38	1.65	1.17
$Q_{numerical}$ (m^3/day)	2.82	2.38	1.65	1.15

Table 2
Comparison of Observed and Predicted Seepage-Face Lengths

Head Gradient	90:20	90:40	90:60	90:70
Observed (cm)	41	26	8	2
Numerical (cm)	40	25	7.5	2.5

Ground Water Discharge Pattern at the Seepage-Face Boundary

The vertical distribution of the horizontal fluid velocity measured in the sand tank ~5 cm upstream from the exit boundary (i.e., r = 15 cm) is shown in Figure 3. Due to the experimental difficulties encountered in measuring the exact fluid velocity, we normalized both the observed data points and the numerical profiles in Figure 3 using their respective maximum fluid velocities. The results, therefore, describe the relative trend in the vertical distribution of the horizontal transport velocity. Several difficulties were encountered in measuring the velocity of the injected slugs close to the outflow boundary; first, it was difficult to physically observe the tracer movement close to the boundary because the steel frame of the model obscured the view. Second, the converging nature of the flow and high fluid velocities introduced large measurement errors. A mild 90:75 gradient was used to minimize some of these experimental difficulties.

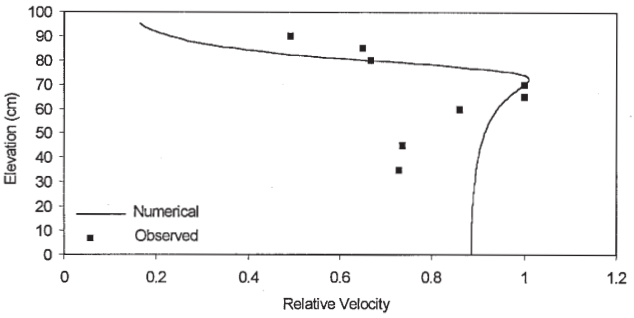

Figure 3. Vertical distribution of horizontal fluid velocity toward the seepage-face boundary.

Results shown in Figure 3 indicate that the horizontal flow velocity reached a maximum at the elevation corresponding to the seepage face at the exit boundary; this trend was clearly observed in the laboratory data and in the predicted numerical profile. The numerical model was used to further analyze the patterns of discharge near the exit boundary. To model the seepage-face zone of the mild 90:75 gradient experiment, the numerical code was rerun with a significantly refined computational grid with Δz set at 0.25 cm. Figure 4 shows the horizontal velocity profiles computed at three internal mesh points located approximately at 3, 5, and 10 cm upstream from the exit boundary (i.e., r = 13, 15, and 20 cm). Although the seepage face for the 90:75 gradient was <1 cm in length, the velocity profiles show a distinct peak near the seepage face. At outflow boundary, the velocity through the seepage-face region is ~30% higher than the velocity at the base of the aquifer.

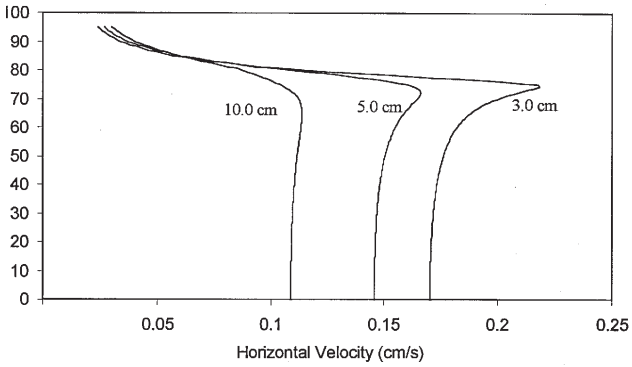

Figure 4. Comparison of horizontal velocity as function of distance away from the seepage-face boundary.

These experimental results highlight the importance of the seepage face in controlling the vertical distribution of fluid discharge near a ground water/surface water interface. Additionally, these observations are important as they physically confirm previous results that were based only upon theoretical analysis. For example, Muskat (1937) used the Hodograph method to demonstrate that the horizontal velocity along the outflow boundary of the regular dam problem is a maximum at the base of the seepage face. Numerical evidence to show that the outward flux is a maximum at the base of the seepage-face boundary has also been presented (Neuman and Witherspoon 1971; Vauclin and Vauchad 1975; Clement 1993). In our laboratory experiments, however, we have made an attempt to physically verify this velocity variation near a seepage-face boundary.

Tracer Transport Experiments

A time series of photographs from tracer experiments are first used to illustrate several key features of the transport patterns in the vicinity of a seepage face. Figure 5

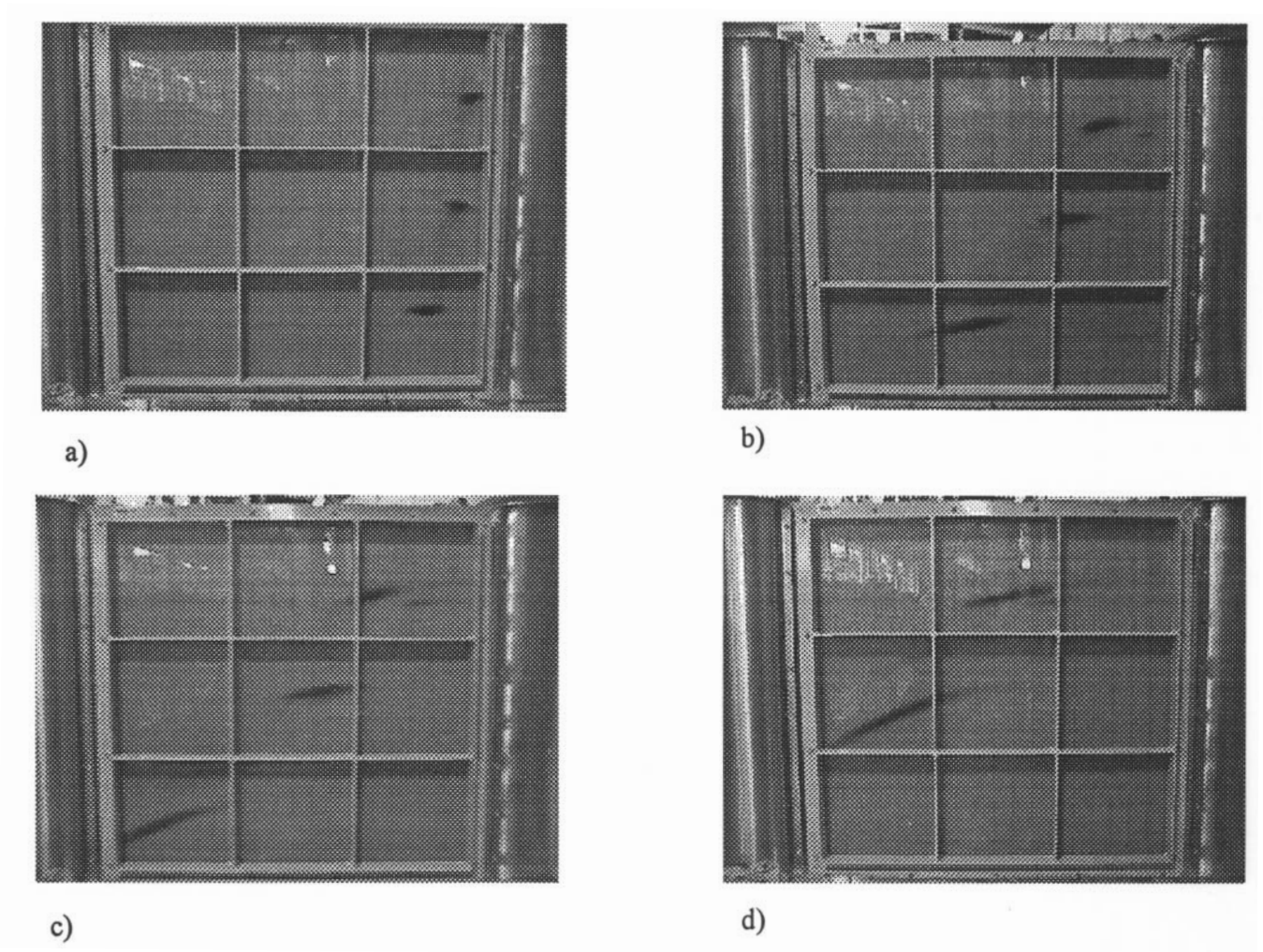

Figure 5. Tracer slug transport after (a) 5 minutes, (b) 15 minutes, (c) 20 minutes, and (d) 25 minutes.

shows a qualitative illustration of the transport patterns observed in the laboratory tank for the 90:20 gradient experiment. Three dye slugs were injected at elevations of 20, 45, and 75 cm and four photographs were taken at 5, 15, 20, and 25 minutes after the injection. As shown in the figures, after 15 minutes of transport, the slug released closest to the base of the aquifer had moved significantly farther than the other two. After 20 minutes, the bottom slug had reached the outflow boundary, and after 25 minutes the bottom slug has completely exited the outflow boundary while the middle slug had just arrived at the outflow boundary. These results are in agreement with those results reported in the previous section, where we observed that the outflow velocity was a maximum at the elevation corresponding to the base of the seepage face. For the 90:20 gradient experiment, the maximum outflow velocity is therefore expected to occur at an elevation of 20 cm. This is consistent with the observations in Figure 5, where the dye slug released at an elevation of 20 cm moved relatively faster than the other two slugs.

These experimental observations have several important implications. The tracer-transport data show that the solute-transport patterns near a seepage-face boundary are strongly influenced by the three-dimensional flow characteristics of the system. Therefore, vertically averaged flow models that employ Dupuit approximations may introduce considerable error in a localized solute transport analysis. These errors could further be magnified if bio/geochemical reactive transport processes control the fate of solutes through this transition zone. The consideration of solute residence times near seepage faces are important as these fringes of surface water bodies are known to be critical buffer zones which generally support important microbial processes such as denitrification (Tobias et al. 2001). Therefore, models that ignore seepage faces may incorrectly predict the residence time distribution of the nutrients through this buffer zone, and hence may predict erroneous nutrient concentration levels. In light of these results, it appears that a detailed three-dimensional flow model, which accounts for vertical flow and seepage-face formation processes, might be required to accurately predict solute transport near a ground water/surface water interface.

In the following discussion, we report several sets of tracer transport experiments that are used to quantitatively verify the capability of the three-dimensional, axi-symmetric, numerical flow model to describe the transport patterns near a seepage-face boundary. Experiments were conducted to quantify the solute transport travel time distribution under three different hydraulic gradient conditions. For each of the imposed hydraulic gradients, the time required for several slugs of dye to traverse a 90 cm horizontal flowpath was measured. Five slugs were injected at the elevations of 90, 75, 60, 45, and 15 cm along a vertical plane where r = 105 cm. The time required for the slug to cross the vertical plane where r = 15 cm was then recorded. Only the middle portion of the tank, from r = 105 cm to r = 15 cm with a total horizontal travel distance of 90 cm, was used to conduct these travel time experiments. The total measured travel time along with the numerically predicted travel time required for several dye slugs to traverse the aquifer in a 90:40 gradient experiment is presented in Figure 6. Several interesting observations can be made from the figure. First, the measured travel times depend on the depth at which the dye slug was released. This dependence stems from the fact that the dye particles released at higher elevations required a longer time to traverse the tank, partly because they were transported along curved flowpaths and partly because of the variation in fluid velocities along those paths. Note that the maximum fluid velocity along the outflow face is expected to occur at an elevation of 40 cm, corresponding to the base of the seepage face. Second, it is clear that the three-dimensional, axi-symmetric, numerical flow model is capable of predicting the travel time distribution within the aquifer with some degree of certainty.

It can be observed from Figure 6 that the numerical model results compare well with most of the observed data points, except for the 90 cm release point. The discrepancy in the travel time for this point is, to some extent, caused by experimental errors. Note that this point is adjacent to the unsaturated zone in the physical model; as the slug dispersed, a portion of the slug interacted with the unsaturated zone and was affected by the reduced fluid flux within the unsaturated zone. Therefore, it became increasingly difficult to identify the center of mass of this slug and this resulted in large experimental errors.

To further investigate the travel time trends, two extreme variations on the original 90:40 gradient experiment were made. First, a 90:20 gradient experiment was completed to observe the transport under an extremely high gradient condition; and second, a 90:60 gradient experiment was completed to observe the transport under a relatively mild gradient condition. Similar to the 90:40 experimental results, the measurements from the 90:20 and 90:60 gradient experiment show that the numerical model was able to capture the travel time trends quite well (Figures 7 and 8). The dye slug released at 90 cm was once again affected by unsaturated flow conditions and encountered problems similar to those explained in the previous experiment. There are also some interesting observations to be made between the data shown in Figures 6, 7, and 8. First, the average travel time is longer for the milder gradient case. This is an intuitive result because weaker hydraulic gradients are expected

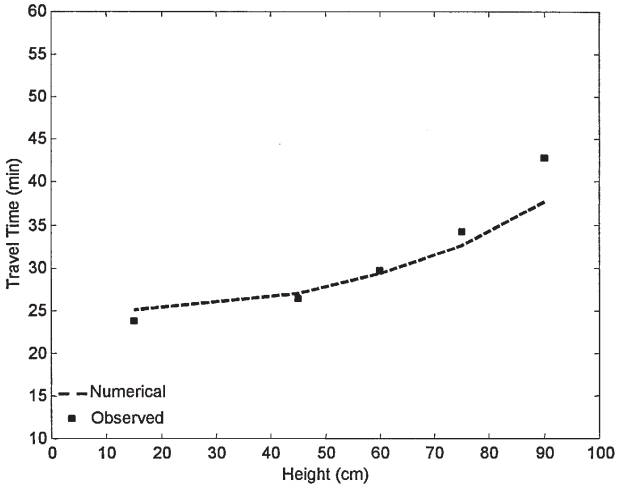

Figure 6. Observed and predicted travel times for the 90:40 gradient experiment.

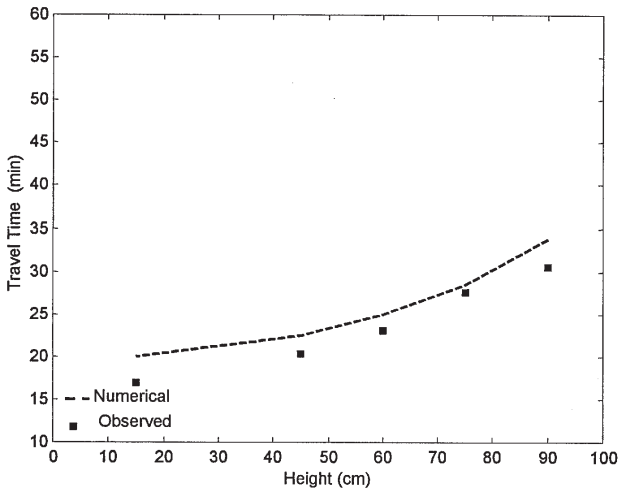

Figure 7. Observed and predicted travel times for the 90:20 gradient experiment.

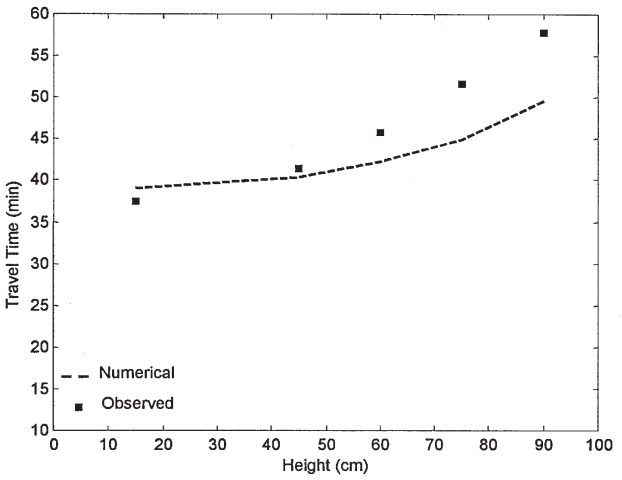

Figure 8. Observed and predicted travel times for the 90:60 gradient experiment.

to induce smaller fluid velocities. Second, the travel time results for the 90:20 gradient exhibit a stronger dependence on the depth at which the slug was released when compared to the 90:40 and 90:60 case. For example, the numerical results indicate that the maximum difference in the residence time of a particle released at the top of the aquifer compared to that for a particle released at the base of the aquifer for the 90:20 gradient is ~14 minutes. In comparison, the numerical results show that for the 90:60 gradient there is only a 10-minute difference between the residence times at the top and base of the aquifer. This implies that the three-dimensional transport effects are greater for the 90:20 gradient experiment.

Another point of interest is in the relative difference between the predicted travel-time profiles and measured travel-time data under different gradient conditions. For example, with the exception of the 90 cm data point, both the 90:40 and 90:20 profiles show a good correspondence between the numerical and observed data points. However, the 90:60 gradient observed travel times are consistently higher than the numerical results. This was because the average travel time for the weaker 90:60 gradient experiment was much longer than other experiments and therefore the dye slugs were subjected to greater spreading by dispersion. This increase in spreading made the measurement of the center of mass of the slugs to be progressively more difficult. Hence, the experimental data collected under the weaker gradient condition have a larger uncertainly. This explains in part, the divergence of the observed travel times from the predicted numerical profiles as the hydraulic gradient across the system was decreased.

Analysis of Observed Streamline Data

The hydraulic gradient for these experiments was fixed at the 90:20 level. A slug of dye was released at an upstream point and the location of the center of mass of the slug was recorded at each 5 cm horizontal increment as the slug was transported through the aquifer. The experiment was repeated five times by changing the elevation of the upstream release point. A similar transport experiment was also simulated using the numerical model. A comparison of the observed and predicted streamlines is shown in Figure 9.

An important transport feature that could be observed in the 90:20 experiment is that the bulk of the outflow occurred through the 40 cm long seepage-face boundary. Although the exit water level is fixed at 20 cm, the tracer discharge into the well is distributed over a 60 cm long exit face. The observed streamlines imply that seepage faces could play a dominant role in transmitting water and associated dissolved solutes across the ground water/suface water boundary. This exercise also shows that under the 90:20 gradient condition, the spatial distribution of the solutes within the aquifer is dominated by the seepage-face dynamics. It can be inferred from the data that any particle released above an elevation of 25 cm at the upstream boundary exits through the seepage face; therefore, the seepage-face zone is a major capture zone in this problem. These results show that under such strong gradient conditions it is impossible to meaningfully predict the spatial distribution of solutes without appropriate consideration of the seepage-face boundary. These types of seepage-face controlled flow regimes can occur when bank storage processes dominate the water balance of a riparian zone. The phenomenon of bank storage happens when a large surface water runoff event occurs in a

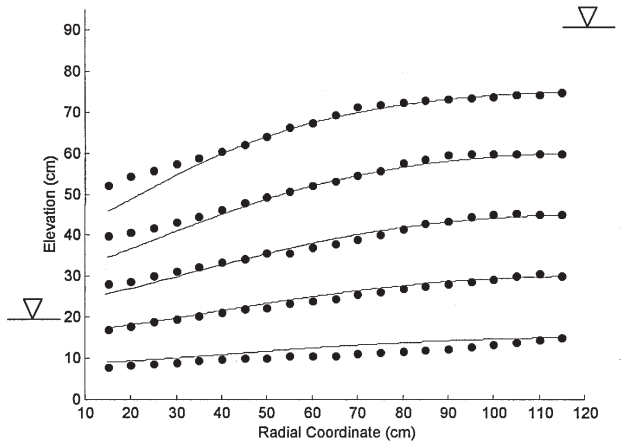

Figure 9. Streamlines for 90:20 hydraulic gradient experiment: numerical streamlines (solid line), observed data (data points).

stream channel. As the runoff migrates through the channel, the water levels rise causing a subsurface flow into the surrounding bank sediments. The water is temporarily stored in the bank sediments and will be released back into the channel as the surface water elevation drops to its equilibrium position. This transfer occurs through a large seepage-face boundary formed under strong hydraulic gradient conditions (Whiting and Pomeranets 1997). Therefore, the implications of the laboratory observations could be useful for developing a fundamental understanding of the local ground water and solute transport processes through a ground water/stream interface.

Conclusions

The dynamics of ground water flow and solute transport near a seepage face were analyzed through the use of a radial soil tank model and a three-dimensional, axi-symmetric, numerical model. The physical model was used to observe the fluid flow and transport characteristics for a range of hydraulic gradients. The flow analysis was characterized in terms of total discharge, exit-face discharge distribution, and seepage-face length; and the solute transport analysis was characterized by recording travel times and streamlines. Several physical observations have been made to directly quantify the transport patterns close to a seepage-face boundary.

The transport experiments conducted near the exit boundary demonstrated the existence of three-dimensional flow characteristics near the seepage face. These results imply that vertically averaged flow models that employ Dupuit approximations might introduce error in the localized analysis of solute transport near a seepage-face zone. Numerical models that ignore seepage faces could also incorrectly predict the residence time distribution. These errors can be further magnified if the transition zone is dominated by biologically mediated reactions.

Comparison of laboratory and numerical modeling results showed that the three-dimensional axi-symmetric numerical model presented in this work can predict the observed flow and transport patterns. Both the physical observations and the modeling results demonstrate that seepage-face boundaries can play an important role in influencing the localized flow-and-solute transport processes of unconfined systems that are dominated by strong hydraulic gradients. Therefore, careful consideration should be given to this boundary condition, particularly when the temporal and spatial distribution of solutes near a ground water/surface water boundary is of interest. The experimental dataset produced in this study will also be of interest for those who are attempting to validate a numerical algorithm for solving ground water flow and solute transport near a seepage-face boundary.

Acknowledgments

The authors are grateful for the comments from the *Ground Water* reviewers: H. Haitjema, B. Kueper, and D. Rogers. In addition, we appreciated the initial review of the work by D.A. Reynolds. This work was made possible by the support provided by the Australian Postgraduate Award system through the Centre for Water Research and the University of Western Australia. This article was, in part, completed when Dr. Clement was at Auburn University.

References

Bear, J. 1972. *Dynamics of Fluids in Porous Media.* New York: Elsevier Publishing Company.

Boulton, N.S. 1951. The flow pattern near a gravity well in a uniform water-bearing medium. *Journal of the Institution of Engineers* 36, 534–550.

Celia, M.A., E.T. Bouloutas, and R.L. Zarba. 1990. A general mass-conservative numerical solution of the unsaturated flow equation. *Water Resources Research* 26, 1483–1496.

Chapman, T.G. 1957. Two-dimensional ground-water flow through a bank with vertical faces. *Geotechnique* 7, 35–40.

Clement, T.P. 1993. Numerical modeling of variably-saturated groundwater flow problems with seepage-face boundaries, Ph.D. dissertation, Auburn University.

Clement, T.P., W.R. Wise, and F.J. Molz. 1994. A physically based, two dimensional, finite difference algorithm for modeling variably saturated flow. *Journal of Hydrology* 161, 71–90.

Clement, T.P., W.R. Wise, F.J. Molz, and M. Wen. 1996. A comparison of modeling approaches for steady-state unconfined flow. *Journal of Hydrology* 181, 189–209.

Clement, T.P. RT3D: A modular computer code for simulating reactive multi-species transport in 3-dimensional groundwater aquifers. Battelle Pacific Northwest National Laboratory Research Report, PNNL-SA–28967, September 1997. Available at: http://bioprocess.pnl.gov/rt3d.htm.

Cooley, R.L. 1983. Some new procedures for numerical solution of variably saturated flow problems. *Water Resources Research* 19, 1271–1285.

Güven, O., F.J. Molz, J.G. Melville, S.E.I. Didy, and G.K. Bowman. 1992. Three-dimensional modeling of a two-well tracer test. *Ground Water* 30, no. 6: 945–957

Haitjema, H.M. 1995. *Analytic Element Modeling of Groundwater Flow.* San Diego: Academic Press.

Hall, H.P. 1955. An investigation of steady flow toward a gravity well. *La Houille Blanche* 10, 8–35.

Hauxwell, A.M., C. Neill, I. Valiela, and K.D. Kroeger. 2001. Small-scale heterogeneity of nitrogen concentrations in groundwater at the seepage face of Edgartown Great Pond. *Biology Bulletin* 201, 290–292.

Keady, G., J. Knight, and G. Williams. 1988. The rectangular dam problem: A survey. *Research Report: Centre for Mathematical Analysis.* Canberra, Australia: Australian National University.

Lee, K.K., and D.I. Leap. 1997. Simulation of a free-surface and seepage face using boundary-fitted coordinate system method. *Journal of Hydrology* 196, 297–309.

Liggett, J.A., and P.L.F. Liu, 1983. *The Boundary Integral Equation Method for Porous Medial Flow.* London: George Allen and Unwin.

Luthin, J.N., and P.R. Day, 1955. Lateral flow above a sloping water table. *Soil Science Society of America Proceedings* 19: 406–410.

Mualem, Y. 1976. A new model for predicting hydraulic conductivity of unsaturated porous media. *Water Resources Research* 12, 513–522.

Muskat, M. 1937. *The Flow of Homogeneous Fluids Through Porous Media.* New York: McGraw-Hill.

Neuman, S.P., and P.A. Witherspoon. 1971. Analysis of nonsteady flow with a free surface using the finite element method. *Water Resources Research* 7, 611–623.

Neuman, S.P. 1973. Saturated-unsaturated seepage by finite elements. *Journal of the Hydraulics Division, Proceedings of the American Society of Civil Engineers.* 99, 2233–2250.

Olivera, I.B., A.H. Demond, and A. Salehzadeh. 1996. Packing of sands for the production of homogeneous porous media. *Soil Science Society of America Journal* 60, 49–53.

Oostrom, M., J.H. Dane, O. Güven, and J.S. Haysworth. 1992. Experimental investigation of dense solute plumes in an unconfined aquifer model. *Water Resources Research* 28, 2315–2326.

Polubarinova-Kochina, P.Y. 1962. *Theory of Groundwater Movement.* (Translated by J.M.R. De Wiest). Princeton, New Jersey: Princeton University Press.

Press. W.H., B.P. Flannery, S.A. Teukolsky, and W.T. Vetterling. 1992. *Numerical Recipes in Fortran: The Art of Scientific Computing*, 2nd edition. Cambridge, New Jersey: Cambridge University Press.

Shamsai, A., and T.N. Narasimhan. 1991. A numerical investigation of free surface-seepage face relationship under steady state flow conditions. *Water Resources Research.* 27, 409–421.

Silliman, S.E., B. Berkowits, J. Simunek, and M.Th. Genuchten. 2002. Fluid flow and solute migration within the capillary fringe. *Ground Water* 40, no. 1: 76–84.

Tobias, C.R., J.W. Harvey, and I. C. Anderson. 2001. Quantifying groundwater discharge through fringing wetlands to estuaries: Seasonal variability, methods comparison, and implications for wetland-estuary exchange. *Limnology and Oceanography* 46, 604–615.

Vachaud, G., and M. Vauclin. 1975. Comments on "A numerical model based on coupled one-dimensional Richards and Boussinesq equations." *Water Resources Research* 11, 506–509.

Vauclin, M., G. Vauchaud, and J. Khanji. 1975. Two dimensional numerical analysis of transient water transfer in saturated-unsaturated soils. *Modeling and Simulation of Water Resources Systems*, ed. G.C. Vansteenkiste. New York: North Holland Publishing.

Van Genuchten, M.Th., 1980. A closed form equation for predicting the hydraulic conductivity of unsaturated soils. *Soil Science Society of America Journal* 44, 892–898.

Waddill, D.W., and J.C. Parker. 1997. Recovery of light, nonaqueous phase liquid from porous media: Laboratory experiments and model validation. *Journal of Contaminant Hydrology* 27, 127–155.

Westbrook, S.J., G.B. Davis, J.L. Rayner, S.J. Fisher, and T.P. Clement. 2000. Initial site characterization of a dissolved hydrocarbon groundwater plume discharging to a surface-water environment. In *Proceedings of Contaminated Site Remediation: From Source Zones to Ecosystems*, ed. C.D. Johnson, 189–196. Melbourne, Australia.

Whiting, P.J., and Pomeranets, M. 1997. A numerical study of bank storage and its contribution to streamflow. *Journal of Hydrology* 202, 121–136.

Wise, W.R., T.P. Clement, and F.J. Molz. 1994. Variably-saturated modeling of transient drainage: Sensitivity to soil parameters. *Journal of Hydrology* 161, 91–108.

Wycoff, R.D., H.G. Botset, and M. Muskat. 1932. Flow of liquids through porous media under the action of gravity. *Physics* 2, 90–113.

Zheng, C., and G.D. Bennett. 2002. *Applied Contaminant Transport Modeling.* New York: John Wiley & Sons.

Appendix A: Variably Saturated Flow Model

The algorithm described by Clement et al. (1994) was used to solve the mixed form of the transient, two-dimensional (vertical) variably saturated flow equation:

$$S_s\frac{\theta}{\theta_s}\frac{\partial\psi}{\partial t} + \frac{\partial\theta}{\partial t} = \frac{\partial}{\partial x}\left[K(\theta)\frac{\partial\psi}{\partial x}\right] + \frac{\partial}{\partial z}\left[K(\theta)\frac{\partial\psi}{\partial z}\right] + \frac{\partial K(\theta)}{\partial z} \quad \text{(A1)}$$

where S_s [L^{-1}] is the specific storage of the medium, θ is the water content, θ_s is the saturated water content (porosity), y[L] is the pressure head, K [LT^{-1}] is the hydraulic conductivity, x [L] and z [L] are the Cartesian coordinates and t [T] is the time.

The numerical solution of Equation A1 by the method of finite-differences was partially described by Clement et al. (1994). The algorithm used for this work was modified from that presented by Clement et al. (1994) in two ways. First, the algorithm was used in a radial coordinate system; second, the algorithm was used to obtain a steady-state solution. Re-expressing Equation A1 in terms of a radial coordinate system yields

$$S_s\frac{\theta}{\theta_s}\frac{\partial\psi}{\partial t} + \frac{\partial\theta}{\partial t} = \frac{1}{r}\frac{\partial}{\partial r}\left[rK(\theta)\frac{\partial\psi}{\partial r}\right] + \frac{\partial}{\partial z}\left[K(\theta)\frac{\partial\psi}{\partial z}\right] + \frac{\partial K(\theta)}{\partial z} \quad \text{(A2)}$$

where r [L] is the radial coordinate and all other terms are previously defined.

The application of the finite-difference approximation to the spatial terms of Equation A2 follows that of the Cartesian system originally described by Clement et al. (1994). The main difference is in how the steady solution is obtained while still using the modified Picard approach (Celia et al. 1990). Typically for the solution of a transient problem, the temporal change in the moisture content term is approximated using the modified Picard approach:

$$\frac{\partial\theta}{\partial t} \approx \left[\frac{\theta_i^{n+1,m} - \theta_i^n}{\Delta t}\right] + C_i^{n+1,m}\left[\frac{\psi_i^{n+1,m+1} - \psi_i^{n+1,m}}{\Delta t}\right] \quad \text{(A3)}$$

where n+1 refers to the current time iteration level, m+1 refers to the current modified Picard iteration level, C_i [L^{-1}] refers to the specific water capacity (gradient of the soil-water-retention curve) at the ith node and Δt [T] is the time step.

The first term on the right side of Equation A3 is an explicit estimate of the partial time derivative of the water content, based on the mth Picard level estimates of the pressure head. In the second term of the right side of Equation A3, the numerator of the bracketed fraction is an estimate of the error in the pressure head at the ith node between two successive Picard iterations. The problem with making the simulation steady-state is that while the temporal derivative of the water content is identically zero under steady conditions, there must be some method of updating the pressure estimates using the modified Picard scheme so that the steady-state pressure profile converges. This is achieved by setting the first term of the right side of Equation A3 to zero and leaving the second term as for the usual unsteady scheme. This means that as the Picard iteration proceeds, the numerator of the second term shall tend to zero as the solution converges, even if the algorithm is supplied with a value for the time step. Therefore, by simply removing the time loop, setting S_s = 0.0, and making the first term on the

right of Equation A3 zero, the original transient scheme outlined by Clement et al. (1994) is conveniently converted into a steady-state algorithm.

The numerical solution of Equation 1 requires the soil water retention function and the unsaturated hydraulic conductivity function of the porous medium. The following van Genuchten (1980) relationship was used to simulate the soil water retention function:

$$\Theta = \left[\frac{1}{1 + (\alpha_v|\psi|)^{n_v}}\right]^{m_v} \quad \text{(A4)}$$

where α_v [L^{-1}], n_v, and $m_v = 1-(1/n_v)$ are the van Genuchten parameters, and Θ is the effective saturation given by the relationship

$$\Theta = \frac{\theta - \theta_r}{\theta_s - \theta_r} \quad \text{(A5)}$$

where θ_s is the saturated water content and θ_r is the residual water content of the soil. Mualem's (1976) model was used to simulate the unsaturated hydraulic conductivity function. Further details of these models and the methods for implementing these models within a variably saturated flow code are summarized in Clement et al. (1994).